RESEARCH ARTICLE



Hybrid femtosecond/picosecond pure-rotational coherent anti-Stokes Raman scattering with chirped probe pulses

Chaobo Yang^{1,2} | David Escofet-Martin² | Derek Dunn-Rankin² | Yu-Chien Chien² | Xin Yu¹ | Shaul Mukamel³

¹National Key Laboratory of Science and Technology on Tunable Laser, Harbin Institute of Technology, Harbin 150001, China

²Department of Mechanical and Aerospace Engineering, University of California, Irvine 92697, CA, USA

³Department of Chemistry, University of California, Irvine 92697, CA, USA

Correspondence

Chaobo Yang, National Key Laboratory of Science and Technology on Tunable Laser, Harbin Institute of Technology, Harbin 150001, China.

Email: peteryang110@gmail.com David Escofet-Martin, Department of Mechanical and Aerospace Engineering, University of California, Irvine 92697, CA, USA.

Email: descofet@uci.edu

Funding information

NSF, Grant/Award Number: CHE-1361516; W. M. Keck foundation

Abstract

The influence of probe laser chirp on hybrid femtosecond/picosecond pure-rotational coherent anti-Stokes Raman scattering is studied theoretically and experimentally. Experiments of N_2 (hybrid fs/ps pure-rotational coherent anti-Stokes Raman scattering) are carried out using an in-house built second harmonic bandwidth compressor, results with different probe chirps of are reported. The experimental spectra are fitted with and without considering probe chirp. Including the chirp improves the fit to experimental spectra at all probe delays. The effect of probe pulse chirp is evaluated through a quantitative analysis of matching residuals.

KEYWORDS

chirping, coherent anti-Stokes Raman scattering, combustion diagnostics, ultrafast nonlinear optics

1 | INTRODUCTION

Coherent anti-Stokes Raman scattering (CARS) is a powerful nonintrusive diagnostic tool of combustion science. This technique is widely used for temperature and species determination because of its high precision and robust applicability in harsh combustion environments. [1-4] Limitations associated with traditional ns-CARS include low repetition rate and interference from nonresonant background signals. Recently, the development of femtosecond (fs) CARS had made it possible to realize kilohertz measurement rates without the complication of a nonresonant background. [5-8] To overcome the low spectral resolution offered by broadband fs lasers, a

hybrid combination of broadband excitation and picosecond (ps) narrowband detection has been developed, and the concept itself dates back to the early 1980s. [9, 10] Hybrid fs/ps pure-rotational CARS (HRCARS) has been successfully used for single-shot temperature and species measurements even under highly sooting hostile environments. [11-14] 1D and 2D imaging with HRCARS for flame thermometry has also been reported. [15-17] The theoretical modeling of HRCARS has been developed, and the effects of pressure, probe pulse shape, and chirp of pump/Stokes pulses were discussed. [12, 18-21]

In this paper, we report a HRCARS experiment of N_2 under room temperature using different probe chirps. Probe chirp effects on HRCARS are investigated by fitting the experimental spectra with our model.

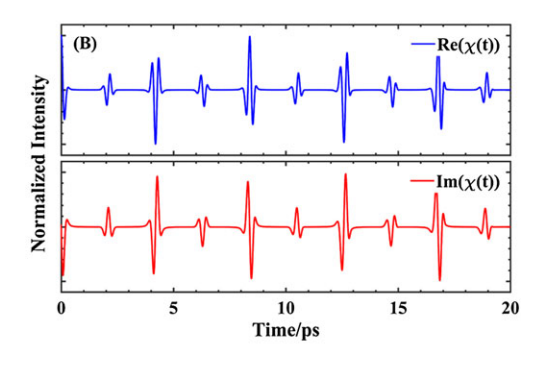


FIGURE 1 (a) Energy level diagram for the hybrid femtosecond/picosecond pure-rotational coherent anti-Stokes Raman scattering. The rotational levels are covered by the broadband femtosecond pulses (ω_1 and ω_2) that performed as pump and Stokes laser. The Raman coherence is probed by the picosecond laser (ω_3) to generate the coherent anti-Stokes Raman scattering (CARS) spectra (ω_4). (b) Theoretical Raman signal of N₂ under 300 K in the time domain. ps = picosecond [Colour figure can be viewed at wileyonlinelibrary.com]

2 | THEORETICAL MODEL

The energy level diagram of HRCARS is presented in Figure 1(a). To prepare the rotational coherence, a broadband fs laser is used to produce a pump (ω_1) and a Stokes (ω_2) pulse that cover several rotational states. After a delay T, the prepared coherence is probed by a ps narrowband probe laser pulse (ω_3) .

The third order polarization is given by^[22]:

$$P_{Res}^{(3)}(t,T) = (\frac{i}{\hbar})^3 E_{probe}(t) \int_0^\infty dt_2 [R(t_2) E_2^*(t+T-t_2) E_1$$

$$(t+T-t_2) \exp[i(\omega_1-\omega_2)t_2]].$$
(1)

The Raman response of N_2 in the time domain is given by^[23]:

$$R(t) = \sum_{\nu} \sum_{\Delta J=2} I_{\nu,JJ'}(T) \exp[(-i\Omega_{\nu,JJ'} - \Gamma_{\nu,JJ'})t]. \tag{2}$$

Here, the summation is taken over populated vibrational levels ν and all the S-branch rotational transitions between J and J' ($\Delta J=2$), which have the Raman wavenumber $\Omega_{\nu,JJ'}$. The Raman linewidth $\Gamma_{\nu,JJ'}$ caused by collisional dephasing is negligible when the probe delay is smaller than the collisional lifetime as is the case for these experiments. $I_{\nu,JJ'}(T)$ are the corresponding Raman transition strengths. Both $\Gamma_{\nu,JJ'}$ and $I_{\nu,JJ'}(T)$ can be calculated with the constants recommended by Martinsson et al. [24] With a Fourier transform from Equation 1, the CARS signal is finally given by:

$$I_{CARS}(\omega, T) = |P_{Res}^{(3)}(\omega, T)|^2.$$
 (3)

The structure of N_2 S-branch Raman transitions is shown in Figure 1(b). The rotational Raman signal exhibits a periodic structure in time caused by the molecular alignment introduced by the fs pulse. The rephasing angular frequency of each rotational state J is given by $\Omega_J = (1/2)J(J+1)$

1) Ω_1 , where $\Omega_1 = 4\pi B_0 c$ is the fundamental rephasing frequency.^[25] The revival period of the molecular ensemble is given by $\tau_{full} = 2\pi/\Omega_1$. For N₂ ($B_0 = 1.998 \text{cm}^{-1}$), as shown in Figure 1(b), the period τ_{full} is equal to 8.38 ps.

For S-branch pure-rotational Raman transitions, the Raman wavenumber in Equation 2 is given by $\Omega_{\nu,JJ'}=\Omega_{J+2}-\Omega_J$, and during a complete recurrence, the relative phase accumulation is $(4J+6)\pi=0$ (modulo 2π). At the half recurrence, all transitions accumulate a relative phase of $(2J+3)\pi=\pi$ (modulo 2π). But at the quarter recurrence, the accumulated relative phase $(J+3/2)\pi$ is $-\pi/2$ and $\pi/2$ (modulo 2π) for odd J and even J, respectively. There is a similar but reverse situation at $3/4\tau_{full}$. [18] This opposite phasing of odd and even J transitions results in a destructive interference between them. Because N_2 has a 2:1 in the ratio degeneracy factor for even and odd rotational states, this interference will distort the spectra of odd transitions, when the probe pulse is chirped.

We have added probe chirp factor to the model of HRCARS and simulated the spectra at different probe delays. A Gaussian probe pulse with linear chirp can be written as^[26]:

$$E_{probe}(t) = A \exp\left[-\frac{(2 \ln 2)t^2}{t_1^2}\right] \exp\left[-i\frac{(2 \ln 2)\alpha t^2}{t_1^2} - i\omega_0 t\right],$$
(4)

$$t_1^2 = t_0^2 \cdot (1 + \alpha^2),\tag{5}$$

$$\frac{d\omega}{dt} = \frac{2 \cdot (2\ln 2)\alpha}{t_1^2}.$$
 (6)

The probe pulse envelope can affect the CARS signal, so the real part of Equation 4 will be replaced by experimentally determined E(t) in the following fitting of experimental results. In the simulation of N_2 CARS spectra, the duration of Gaussian probe pulse t_1 was set to 3 ps full width at half maximum (FWHM). The chirp factor of the

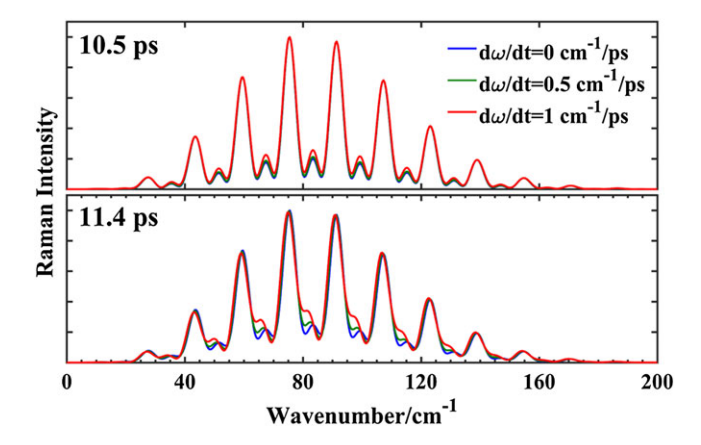


FIGURE 2 Simulation of N_2 (hybrid fs/ps pure-rotational coherent anti-Stokes Raman scattering) at $T = 1/4\tau_{full}$ (10.5 ps) and T = 11.4 ps [Colour figure can be viewed at wileyonlinelibrary.com]

probe pulse $(d\omega/dt)$ was set to 0, 0.5, or 1 (cm⁻¹/ps). With chirp 0.5 and 1 (cm⁻¹/ps), the pulse duration t_1 is 4.7% and 17.2% longer than the transform limited duration t_0 , respectively.

From Equation 3, the simulated normalized HRCARS spectra of N_2 at quarter recurrence ($\tau = 10.5$ ps) and an arbitrary probe delay ($\tau = 11.4$ ps) are shown in Figure 2.

Chirp effects and their variation with the probe delay are clearly visible. For T = 10.5 ps, the center frequency of the transitions between odd rotational states is constant with the change of probe chirp. But for the 11.5 ps probe delay, the center frequency of the transitions has an obvious shift. For these two probe delays, the amplitude ratio between the smaller (odd J) and the larger (even J) peaks changes.

3 | EXPERIMENTAL SETUP

These simulated effects caused by probe pulse chirp were reproduced and verified in the experiments under different probe delays and chirp factors. A home built second harmonic bandwidth compressor (SHBC) was used to generate a ps pulse and change its chirp factor continuously. Several techniques may be used to create a narrowband probe pulse for realizing this hybrid fs/ps CARS setup. [12, 16, 23] To adjust the chirp of the probe pulse continuously, a bandwidth compressor based on the conjugate chirp sum-frequency is selected. The diagram of our HRCARS is shown in Figure 3.

The SHBC is based on the effect reported by Raoult et al.^[27] The design of the SHBC in this paper is the front end of the usual "4f" design of a full stretcher, which is selected because we can achieve a compact and economical stretcher setup with this method. Opposite temporal chirps are introduced to two fs pulses separately and then eliminated by the sum-frequency generation process

between them. Our SHBC instrument is similar to the device reported by Zhu et al.^[28] Two cylindrical lenses with focal length f were used to collimate the beams diffracted by the grating. The lenses placed at $L_1 = f - d_1$ and $L_2 = f + d_2$ introduced positive and negative chirp to the laser, respectively. When the detuning d_1 and d_2 were equal to each other, we produced two laser pulses with precisely conjugate chirps. The sum frequency of these two beams generated a narrowband ps laser. In the experiment, the SHBC is built up with one reflective grating (1,200 grooves/mm, 1,000~nm blaze at 36.8°, 20RG1200—00093;1000-2, Newport). The focal length of cylindrical lenses is 30 cm, and the displacement d_1 and d_2 are about 5 cm. In our SHBC instrument, the ps probe pulse can be generated at 1 kHz with 7 cm⁻¹ bandwidth at around 400 nm. Unfortunately, because of the aberration caused by mirrors and lenses, it is hard to generate a completely chirp-free laser by sum-frequency generation. In this SHBC instrument, by adjusting d_1 , the residual chirp in the probe pulse can be changed continuously.

The probe delay was varied by adjusting a manual translation stage in the optical path of the probe laser. To fully depict the spectra in the recurrence period, the increment of the translation stage was set to 160 microns, which was equivalent to around 1.067 ps ($\sim 1/8\tau_{full}$). The initial probe delay was set to 5.20 ps to avoid contributions from nonresonant signal around 0 ps. Two groups of N2 CARS spectra were obtained under 300 K in the experiment. In the first case, the probe pulse had a 3 ps (FWHM) with ~ 1 cm⁻¹/ps chirp, and for the second, they were 4.3 ps (FWHM) and ~ 1.3 cm⁻¹/ps. The only difference between these two groups was the detuning of the cylindrical lens (d_1) . The two groups of spectra are presented in the upper and lower level of Figure 4, separately. These two groups of experimental data (black solid lines) had an obvious variation with the change of probe delay. Also at the same probe delay, the difference between the two groups was notable, which was consistent with the simulation results from our model.

We had further employed a least-squares optimization algorithm to fit the experimental data. The modified model and the standard model (without chirp) were used to fit these CARS spectra simultaneously. Before the fitting, the CARS spectra of N_2 were pretreated as reported. [12, 20] A signal average was taken after every 100 shots, and I(t) for probe pulses were measured by cross-correlation. During fitting, the probe delay was fixed to the measurement value. Only a shift and stretch of the spectrum on the wavenumber axis was allowed. The chirp factors of our model were obtained from the fitting results of spectra with the first probe delay (5.20 ps). For a fair comparison, these chirp factors were fixed for all the other probe delays. The CARS spectra can be properly fitted with the modified

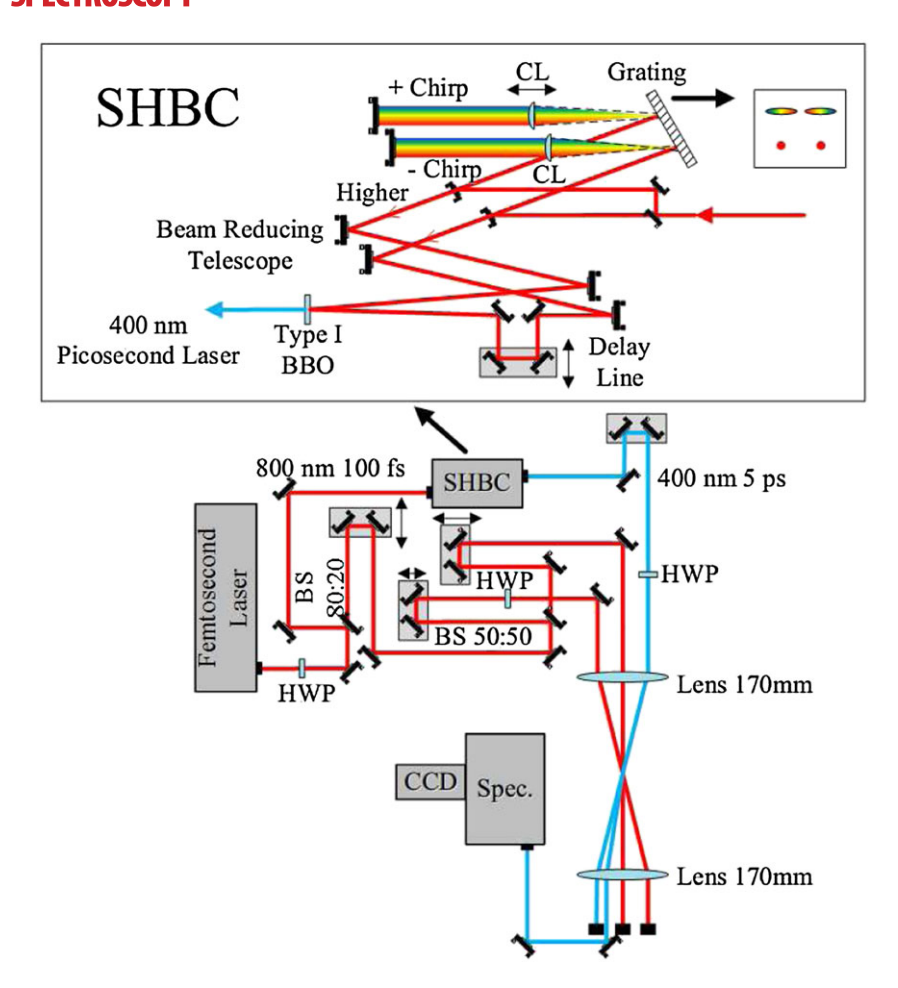


FIGURE 3 Schematic of hybrid fs/ps rotational coherent anti-Stokes Raman scattering with second harmonic bandwidth compressor (SHBC) instrument. The translation stages are indicated by double arrows; cylindrical lens (CL); beam splitter (BS); have-wave plate (HWP). In the SHBC part, the beams output from the stretcher have a higher angle than the input beams to avoid being blocked by the input mirrors. CCD = charge-coupled device; BBO = Beta barium borate [Colour figure can be viewed at wileyonlinelibrary.com]

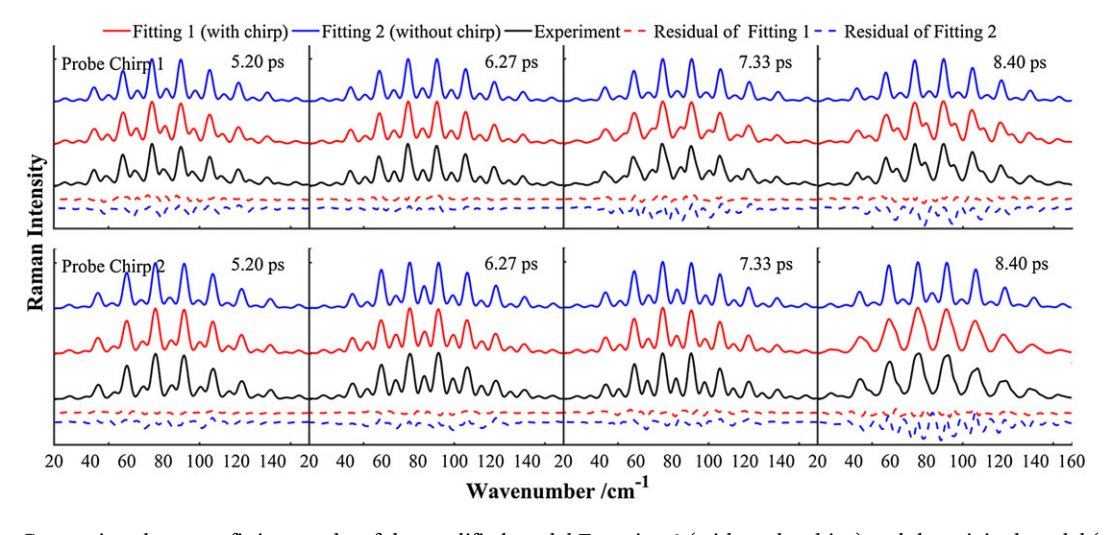


FIGURE 4 Comparison between fitting results of the modified model Equation 3 (with probe chirp) and the original model (without chirp). Two groups of coherent anti-Stokes Raman scattering spectra of N_2 (black solid lines) with different probe chirps are fitted. Fitting results of the model (with and without chirp) are presented [Colour figure can be viewed at wileyonlinelibrary.com]

model. At each probe delay, 100 frames of CARS spectra are acquired and fitted with the modified model. The average relative error of temperature measurement at all the probe delays of both cases is better than 5%. And the discussion of the difference between the fitting with modified model and standard model is presented in following section.

4 | RESULTS AND DISCUSSION

The simulation results are shown in Figure 4 with red solid lines (fitting 1 with chirp) and blue solid lines (fitting 2 without chirp). The figure shows that at all probe delays including the chirp had improved the fit. For the fitting of every probe delay, the residuals with the chirped model (red dash lines) are smaller than those with the original model (blue dash lines). Along the wavenumber axis, the residuals from the modified model fluctuated randomly. However, the blue dash lines of the standard model show a notable periodic structure.

To evaluate the effect of the probe chirps, the first group of data was studied in detail. The absolute values of residuals were summed along the wavenumber axis for each probe delay. The summations of absolute residuals (SAR) of spectra are presented in Figure 5. The SAR of our model (red rings) are smaller than the SAR of the model without chirp (blue squares) at any probe delay. The SAR of the latter model have an apparent period structure. The minimum values of SAR without chirp appear at 1/4 and 3/4 recurrence period (6.27 and 10.53 ps etc.), which are still larger than the SAR with chirp. The maximum values of SAR without chirp appear at the half and full recurrence period of N_2 (8.40 and 12.60 ps etc.).

We have calculated the difference between spectra with and without probe chirp. The summations of these differences are plotted in Figure 5 with a black solid line. In the calculation, we used the measured pulse shape I(t)

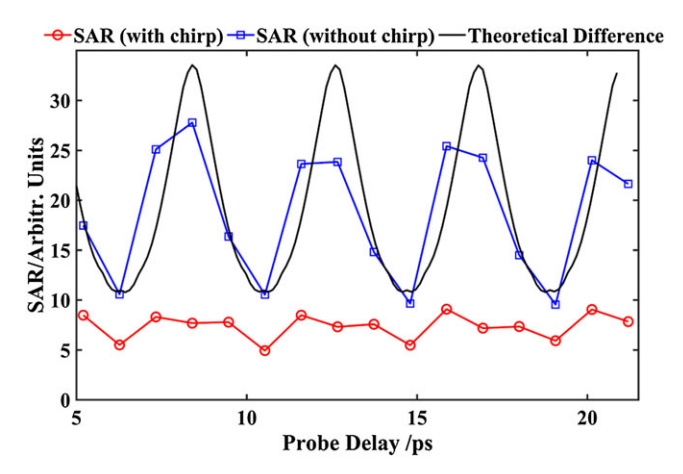


FIGURE 5 Summations of absolute residuals (SAR) from $\tau = 5.20$ to $\tau = 21.20$ ps [Colour figure can be viewed at wileyonlinelibrary.com]

and chirp factor obtained from fitting. Although there is a slight shift in the time axis and a small underestimation at peak points, there is a nice uniformity between SAR without chirp and theoretical difference. This consistency confirms the validity of the influence of probe pulse chirp.

During the fitting process, the least-squares algorithm minimizes the residuals with different fitting parameters. So the inherent SAR of nonchirped spectra will cause a larger fluctuation of fitting parameters. Considering the application background, we fixed all other parameters and only free the temperature to match the SAR of nonchirped fitting. We compared the SAR of nonchirped spectra and spectra under temperature bias, to quantitatively evaluate the effect caused by probe pulse chirp. As presented in Figure 5, there are four peak points and four valley points within the probe delay ranges from 5.20 to 21.20 ps. For the first group of data, an averaged 21 K temperature bias is needed to match the valley values of nonchirped SAR. And for the probe delays of peak values, spectra with 46 K temperature bias is needed to match the SAR of nonchirped spectra. The second group of data has similar results, the temperature bias of valley and peak values are 25 and 57 K, respectively. The SHBC device is prone to induce an unintended chirp so hybird fs/ps CARS thermometry with a SHBC should be conducted with additional caution.

5 | CONCLUSIONS

A chirped probe pulse clearly affects the (HRCARS) spectra in the frequency domain, it shifts and broadens the spectrum in and changes the amplitude ratio between even and odd transitions. This distortion is variable and more significant at some probe delays (half and full recurrence period after molecular alignment). At these probe delays, taking the probe chirp into account is more important.

In combustion thermometry applications, species in the measuring region are more complex than in this ideal monomolecular experiment, so the effects on signals can be complicated. The probe delay should be selected carefully to avoid any crosstalk between Raman responses of multispecies. Pulse chirp effects strongly depend on pulse delay, and it is possible to diminish this dependence for specific delays. In this work, chirp effects are incorporated into the model of HRCARS, and the effects of the probe chirp are effectively modeled. This is of special importance for hybrid fs/ps CARS where the ps probe beam is generated through SHBC due to being more susceptible introduced linear chirp.

ACKNOWLEDGEMENTS

We wish to acknowledge Dr. Sean Kearney from Sandia National Lab. The communication with him was enlightening and helpful for this paper. Support of this work from the W. M. Keck foundation for the study of high pressure combustion is appreciated. S. M. gratefully acknowledges the support of NSF (Grant CHE-1361516).

ORCID

Chaobo Yang http://orcid.org/0000-0001-6324-9792

REFERENCES

- [1] A. C. Eckbreth, Laser Diagnostics for Combustion Temperature and Species, CRC Press, Amsterdam 1996.
- [2] S. Roy, J. R. Gord, A. K. Patnaik, Prog. Energy Combust. Sci. 2010, 36(2), 280.
- [3] F. Vestin, P. E. Bengtsson, Proc. Comb. Inst. 2009, 32(1), 847.
- [4] T. R. Meyer, S. Roy, R. P. Lucht, J. R. Gord, Combust. Flame 2005, 142(1), 52.
- [5] P. Beaud, H-M. Frey, T. Lang, M. Motzkus, Chem Phys Lett 2001, 344(3), 407.
- [6] R. P. Lucht, S. Roy, T. R. Meyer, J. R. Gord, Appl. Phys. Lett. 2006, 89(25), 251112.
- [7] S. Roy, P. J. Kinnius, R. P. Lucht, J. R. Gord, Opt. Commun. 2008, 281(2), 319.
- [8] S. Roy, W. D. Kulatilaka, D. R. Richardson, R. P. Lucht, J. R. Gord, Opt. Lett. 2009, 34(24), 3857.
- [9] W. Zinth, M. C. Nuss, W. Kaiser, Chem. Phys. Lett. 1982, 88(3), 257
- [10] W. Zinth, M. C. Nuss, W. Kaiser, Opt. Commun. 1983, 44(4), 262.
- [11] B. D. Prince, A. Chakraborty, B. M. Prince, H. U. Stauffer, J. Chem. Phys. 2006, 125(4), 044502.
- [12] S. P. Kearney, Combust. Flame 2015, 162(5), 1748.
- [13] S. P. Kearney, D. R. Guildenbecher, Appl. Opt. 2016, 55(18), 4958.
- [14] J. D. Miller, C. E. Dedic, S. Roy, J. R. Gord, T. R. Meyer, Opt. Express 2012, 20(5), 5003.

- [15] A. Bohlin, C. J. Kliewer, J. Chem. Phys. 2013, 138(22), 221101.
- [16] A. Bohlin, C. J. Kliewer, Appl. Phys. Lett. 2014, 105(16), 161111.
- [17] J. D. Miller, M. N. Slipchenko, J. G. Mance, S. Roy, J. R. Gord, Opt. Express 2016, 24(22), 24971.
- [18] H. U. Stauffer, J. D. Miller, S. Roy, J. R. Gord, T. R. Meyer, J. Chem. Phys. 2012, 136(11), 111101.
- [19] H. U. Stauffer, J. D. Miller, M. N. Slipchenko, T. R. Meyer, B. D. Prince, S. Roy, J. R. Gord, J. Chem. Phys. 2014, 140(2), 024316.
- [20] S. P. Kearney, Appl. Opt. 2014, 53(28), 6579.
- [21] M. Marrocco, Opt. Lett. 2014, 39(16), 4831.
- [22] S. Mukamel, Principles of Nonlinear Optical Spectroscopy, Oxford University Press, Oxford 1999.
- [23] J. D. Miller, M. N. Slipchenko, T. R. Meyer, H. U. Stauffer, J. R. Gord, Opt. Lett. 2010, 35(14), 2430–2432.
- [24] L. Martinsson, P.-E. Bengtsson, M. Aldén, S. Kröll, J. Bonamy, J. Chem. Phys. 1993, 99(4), 2466.
- [25] P. W. Dooley, I. V. Litvinyuk, K. F. Lee, D. M. Rayner, M. Spanner, D. M. Villeneuve, P. B. Corkum, *Phys. Rev. A* 2003, 68, 023406.
- [26] P. K. Upputuri, L. Gong, H. Wang, Opt. Express 2014, 22(8), 9611.
- [27] F. Raoult, A. C. L. Boscheron, D. Husson, C. Sauteret, A. Modena, V. Malka, F. Dorchies, A. Migus, Opt. Lett. 1998, 23(14), 1117.
- [28] L. Zhu, W. Liu, C. Fang, Appl. Phys. Lett. 2014, 105(4), 041106.

How to cite this article: Yang C, Escofet-Martin D, Dunn-Rankin D, Chine Y-C, Yu X, Mukamel S. Hybrid femtosecond/picosecond pure-rotational coherent anti-Stokes Raman scattering with chirped probe pulses. *J Raman Spectrosc.* 2017;1–6. https://doi.org/10.1002/jrs.5262